Available online at www.sciencedirect.com
SCIENCE DIRECT®
International Journal of Heat and Mass Transfer 49 (2006) 4070–4081
International Journal of HEAT and MASS TRANSFER
www.elsevier.com/locate/ijhmt

Thermal response of a flat heat pipe sandwich structure to a localized heat flux

G. Carbajal [a], C.B. Sobhan [b], G.P. Peterson [a,*], D.T. Queheillalt [c], H.N.G. Wadley [c]

[a] Department of Mechanical, Aerospace and Nuclear Engineering, Rensselaer Polytechnic Institute, 110, 8th Street, Troy, NY 12180, USA
[b] Center for Nanotechnology, Department of Mechanical Engineering, National Institute of Technology, Calicut 673 601, India
[c] Material Science and Engineering Department, University of Virginia, Charlottesville, VA 22904, USA

Received 27 January 2006; received in revised form 30 March 2006
Available online 9 June 2006

Abstract

The temperature distribution across a flat heat pipe sandwich structure, subjected to an intense localized thermal flux has been investigated both experimentally and computationally. The aluminum sandwich structure consisted of a pair of aluminum alloy face sheets, a truncated square honeycomb (cruciform) core, a nickel metal foam wick and distilled water as the working fluid. Heat was applied via a propane torch to the evaporator side of the flat heat pipe, while the condenser side was cooled via natural convective and radiative heat transfer. A novel method was developed to estimate experimentally, the heat flux distribution of the torch on the evaporator side. This heat flux distribution was modeled using a probability function and validated against the experimental data. Applying the estimated heat flux distribution as the surface boundary condition, a finite volume analysis was performed for the wall, wick and vapor core regions of the flat heat pipe to obtain the field variables in these domains. The results were found to agree well with the experimental data indicating the thermal spreading effect of the flat heat pipe.

Keywords: Flat heat pipe; Thermal spreader; Heat transfer; Evaporator; Condenser

1. Introduction

The use of heat pipes as heat transport devices and heat spreaders has found widespread application in many industries over the past several decades [1–4]. As a result, numerous technical publications, focusing on many aspects of heat pipe design and operation have appeared in the literature [5–8]. Designs have been optimized using theoretical models of heat pipes that range from thermal resistance models and simplified one-dimensional models, to those consisting of coupled sets of highly non-linear, partial differential equations describing the heat and fluid flow in all regions of the heat pipe system. To obtain solutions to these heat and fluid flow problems, various analytical and numerical techniques have been applied. A relatively recent review of both heat pipe modeling and applications can be found in [9].

Although many of the recently reported investigations pertain to the analysis of heat pipes used as heat sinks and thermal spreaders for electronic cooling applications [10–13], some of the research has focused on the analysis of large heat pipes. One of the earliest papers on the flow field analysis of heat pipes was presented by Van Ooijen and Hoogendoorn [14], in which the vapor core of a flat heat pipe was analyzed. Faghri [15,16] has performed numerical studies on vapor flow in concentric double walled heat pipes. Chen and Faghri [17] numerically analyzed the effects of single and multiple heat sources using a model which included wall conduction and the effects of vapor compressibility. Issacci et al. [18] used a two-dimensional numerical model to analyze the start-up process of flat heat pipes. Jang et al. [19] analyzed the transient

* Corresponding author. Tel.: +1 518 2766487; fax: +1 518 2764061.
E-mail address: petersb@rpi.edu (G.P. Peterson).

0017-9310/$ - see front matter © 2006 Elsevier Ltd. All rights reserved.
doi:10.1016/j.ijheatmasstransfer.2006.03.035

Nomenclature

A	area, m^2
c	specific heat per unit volume, $J/(m^3\,K)$
C	specific heat, J/(kg K)
C_E	Ergun's constant, 0.55
F	non-linear function in Eq. (22)
f	friction factor in the porous media
G	linear approximation function (Eq. (23))
g	gravitational constant, m/s^2
h	convection heat transfer coefficient, $W/(m^2\,K)$
h_{fg}	latent heat of vaporization, J/kg
H	flat heat pipe height, m
j	rate of evaporation/condensation (Eq. (19))
K	permeability, m^2
k	thermal conductivity, W/(m K)
m''	mass flux, $kg/(s\,m^2)$
P	pressure, Pa
Q	net heat transfer, J
q	heat transfer rate, W
q''	heat flux, W/m^2
r	capillary radius, m
R	vapor gas constant, J/(kg K)
Re_K	Reynolds number based on the permeability, $\rho_l u_w K^{1/2}/\mu_l$
t	time, s
T	temperature, K
u	x-velocity component, m/s
v	y-velocity component, m/s
v_{fg}	specific volume, $v_g - v_f$, m^3/kg
V	volume, m^3
W	flat heat pipe width, m
x	axial direction, axial distance, m
y	width direction, width, m

Greek symbols

Γ	convective terms
δ	thickness, m
ε	emissivity
θ	the angle between the liquid–vapor interface and solid surface
μ	dynamic viscosity, Pa s
ρ	density, kg/m^3
σ	Stefan–Boltzmann constant, 5.67×10^{-8} $W/(m^2\,K^4)$
σ_R	surface tension, N/m
$\hat{\sigma}$	accommodation factor (Eq. (19))
υ	kinematics viscosity, m^2/s
φ	porosity
Ψ	thermodynamic property function, J/kg

Subscripts

c	condenser
conv	convection
e	evaporator
eff	effective
exp	experimental
f	stationary condition
i	liquid–vapor interface
in	inlet
j	index notation; $j = 1,2$ represent x and y-coordinates respectively
l	liquid
m	mean
num	numerical
o	initial (reference) value
out	outlet
rad	radiation
s	wall material
v	vapor
w	wick material
x	width direction
y	axial direction
∞	ambient conditions

compressible flow of vapor using a one-dimensional model, and compared the results with experimental data. Tournier and El-Genk [20] presented a transient two-dimensional heat pipe analysis model. Wang and Vafai [21] used analytical models to predict the transient performance of a flat plate heat pipe during startup and shutdown processes. Zuo and Faghri [22] presented a network thermodynamic analysis of heat pipes. Vadakkan et al. [23] numerically investigated the transient performance of flat plate heat pipes for large input heat fluxes and highly effective wick thermal conductivity values. An experimental and theoretical approach for the transient behavior of flat plate heat pipes was developed by Xuan et al. [24], where the effects of variations in the amount of the working fluid, thickness of the porous medium and orientation on the performance of flat plate heat pipes were all independently investigated. Only a limited number of investigations have addressed the analysis of the early transient performance of flat heat pipes, making the information pertaining to the relatively large period of time required for these devices to reach steady-state operation, very limited.

The current investigation explores the numerical modeling of the thermal characteristics of a novel sandwich panel heat plate which uses a periodic cellular metal core and solid face sheets to provide structurally efficient load support in bending. The core serves a second function, providing support for a wick that is partially filled with a fluid. The resulting system offers multifunctional opportunities for simultaneous thermal spreading and mechanical load support and might find application in many areas including heating surfaces, electronic cooling modules and near the leading edges of hypersonic vehicles [25].

Here, a large flat heat pipe designed to dissipate high input heat fluxes concentrated on a portion of the evaporator is investigated. Governed by the intended use of this system, it is almost always in the transient state; therefore an explicit finite difference procedure was used to solve the transient governing equations.

1.1. The physical model

The physical dimensions and the thermophysical properties of the flat heat pipe wall material and working fluid of the flat heat pipe are shown in Tables 1 and 2, respectively. Fig. 1 shows a schematic illustration of the heat flux distribution applied to the evaporator surface of the thermal spreader. The reader is referred to Ref. [25] for details of the experimental set up. The flat heat pipe was locally heated for a period of 30 s using a propane torch. Due to the lack of expressions for representing the heat flux distribution of a flame on a flat surface, a numerical study was first performed to obtain this input heat flux. A one-dimensional non-uniform heat flux model was imposed on the evaporator surface in the analysis of the flat heat pipe.

Table 1
Physical dimensions of the flat heat pipe

Width (W), m	0.06350
Height (H), m	0.55880
Wall thickness (δ_s), m	0.00635
Wick thickness (δ_w), m	0.00220

Table 2
Thermophysical properties of the working fluid and the flat heat pipe material at 37.8 °C (values assumed to be constant throughout the analysis)

Physical properties	Liquid (Water)	Vapor (Water)	Solid wall
Density, kg/m^3	996.7	0.04576	2700
Specific heat, J/(kg K)	4183	1420	908
Thermal conductivity, W/(m K)	0.5969	0.01943	237.3
Viscosity, Pa s	8.7×10^{-4}	1.024×10^{-5}	–

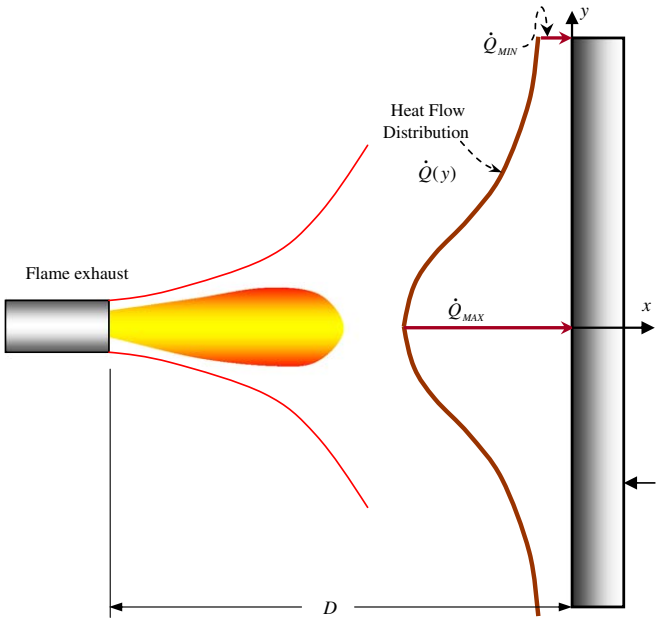

Fig. 1. Schematic diagram of the flat heat pipe under analysis.

For modeling purposes, the transient heating began at $t = 0$ s and persisted at a constant flux for approximately 30 s, after which the heat flux was abruptly decreased to zero. Natural convective cooling was assumed at the condenser side, with an estimated heat transfer coefficient of $\sim$5 W/ (m^2 K). Radiative heat transfer was also accounted for (at the condenser side) in the calculation. The cold surface was painted black, and modeled as a black body, with an emissivity of unity. Temperature measurements were made at the condenser plate using infrared thermal imaging, with an estimated error margin of $\pm$0.5 °C.

Stochastic open-cell nickel foam was used as the wick material due to its high permeability and porosity, and resulted in a substantial reduction in the pressure drop in the fluid flow. Additionally, the solid ligaments in the foam material are mechanically connected to the wall which increases the effective thermal conductivity of the system [26]. The model developed and presented here is intended to analyze the transient thermal performance of such a flat heat pipe and to evaluate the variations of temperature, pressure and velocity fields in the system during the initial transient phase.

1.2. Problem formulation

The flat heat pipe has a large mass, and was subjected to a transient heating condition, where a considerable portion of the applied heat is stored in the body of the flat heat pipe, during its operation (high thermal capacity). The analysis was based on the transient fluid flow and heat transfer governing equations in order to understand the transient behavior. The analysis is aimed at obtaining the distributions of the velocity and temperature in the domain by solving the appropriate governing equations, thereby not requiring any simplifying assumptions such as that of a uniform vapor temperature (as sometimes used in the literature); which is not physically justifiable since the present problem deals with a highly transient condition.

The density field in the vapor varies with respect to time, due to mass addition at the evaporator and mass depletion at the condenser, within the calculation domain. This effect was incorporated into the model by formulating the problem using the continuity equation, solved simultaneously with the transient momentum and energy equations in the field, written in the conservative form, as suggested in the literature [23]. The thermal conductivity, specific heat and dynamic viscosity were all assumed to be constant and the porous medium (the saturated wick) was assumed

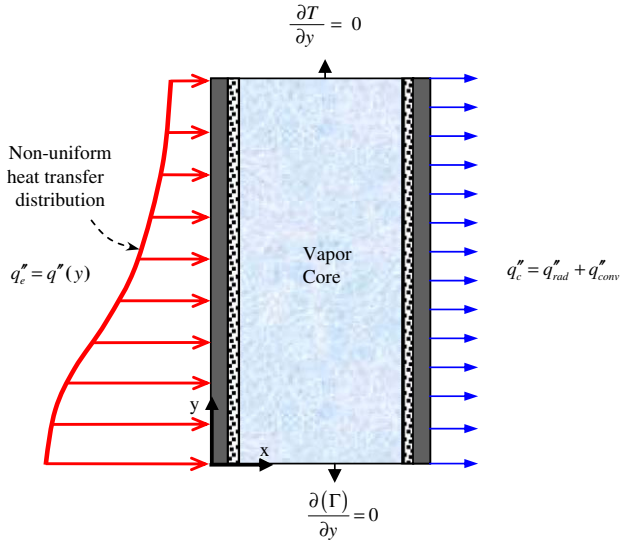

Fig. 2. The domain of analysis and the boundary conditions.

to be isotropic, with constant permeability ($K = 10^{-7}\ \mathrm{m}^2$) and porosity ($\varphi = 0.9$).

The complete mathematical model for the problem is described below, along with the domain of the analysis and the boundary conditions. Due to the symmetry of the problem in the y-direction, the height of the domain of computation is taken as half of the physical domain (see Fig. 2). The formulation involves the governing differential equations in the flow field, the conditions at the physical boundaries of the domain and the mass flux evaluated at the wick-vapor core interface, which is detailed in the following section.

2. The governing equations

2.1. Energy equation in the wall

The governing energy equation in the wall is the two-dimensional unsteady heat conduction equation

$$\rho_s C_s \frac{\partial T}{\partial t} = \nabla.(k_s \nabla T). \tag{1}$$

2.2. Governing equations of the wick

Assuming incompressible flow, the mass conservation in two dimensions can be expressed as:

$$\frac{\partial u_l}{\partial x} + \frac{\partial v_l}{\partial y} = 0. \tag{2}$$

The fluid flow in the wick was analyzed using the extended momentum equations for a porous medium. In the standard form, the augmented Navier–Stokes equations with the Darcy, Brinkman and Forchheimer terms are utilized in the analysis of the fluid flow in porous media [27]. In the present formulation, an additional term is incorporated in the extended momentum equations for the porous medium, which has its basis in the differential statement of the Young–Laplace equation. This takes into account the effect of the change in the size of the capillary radius along the liquid–vapor interface. For a flat surface and constant capillary radius this term becomes zero, i.e., the last term in Eqs. (3), (4). In the case of varying capillary radius, Peterson [28] has observed that the difference in the radii of curvature causes a pressure difference and consequently pumps the liquid from a region with a large capillary radius (condenser) back to a region with a low capillary radius (evaporator).

The extended two-dimensional momentum equations for the computation of the x and y-velocity components in the porous wick are, respectively:

$$\varphi_w^{-1}\left(\frac{\partial u_l}{\partial t} + u_l\frac{\partial u_l}{\partial x} + v_l\frac{\partial u_l}{\partial y}\right) = g_x - \frac{1}{\rho_l}\frac{\partial p_l}{\partial x} + \frac{\upsilon_l}{\varphi_w}\nabla^2 u_l - \frac{\upsilon_l}{K}u_l - \frac{C_E}{K^{0.5}}|\vec{V}_l|u_l - \frac{2\sigma\cos\theta}{r^2\rho_l}\nabla r\cdot\nabla x, \tag{3}$$

$$\varphi_w^{-1}\left(\frac{\partial v_l}{\partial t} + u_l\frac{\partial v_l}{\partial x} + v_l\frac{\partial v_l}{\partial y}\right) = g_y - \frac{1}{\rho_l}\frac{\partial p_l}{\partial y} + \frac{\upsilon_l}{\varphi_w}\nabla^2 v_l - \frac{\upsilon_l}{K}v_l - \frac{C_E}{K^{0.5}}|\vec{V}_l|v_l - \frac{2\sigma\cos\theta}{r^2\rho_l}\nabla r\cdot\nabla x. \tag{4}$$

Paek et al. [26] proposed an empirical correlation for the pressure drop in the foam material. This expression uses the friction factor as a function of the Reynolds number based on the permeability:

$$f = \frac{1}{\mathrm{Re}_K} + 0.105. \tag{5}$$

Based on the empirical correlation given in Eq. (5), the pressure drop in the foam material is computed as follows:

$$\frac{\mathrm{d}p}{\mathrm{d}x_j} = -f_j\frac{\rho_l u_j^2}{K^{1/2}}. \tag{6}$$

The energy equation in the wick, for computing the temperature field is given by:

$$c_m\frac{\partial}{\partial t}(T) + c_l\vec{V}\cdot\nabla T = \nabla\cdot(k_{\mathrm{eff}}\nabla T), \tag{7}$$

where the effective thermal conductivity of the wick is calculated by the correlation proposed by Bhattacharya et al. [29] for metal foams:

$$k_{\mathrm{eff}} = \Lambda[\varphi_w k_f + (1-\varphi_w)k_s] + (1-\Lambda)\left(\frac{\varphi_w}{k_f} + \frac{1-\varphi_w}{k_s}\right)^{-1}. \tag{8}$$

The best fit value for Λ was found to be 0.35 [29]. The mean specific heat, c_m is calculated as suggested by Bejan [30] as follows:

$$c_m = (1-\varphi_w)\rho_s C_s + \varphi_w\rho_l C_l. \tag{9}$$

2.3. Vapor core

As previously explained, the conservative forms of the governing equations are used for the computation in the

vapor domain. The continuity equation used for computing the vapor density field is given by:

$$\frac{\partial \rho_v}{\partial t} + \frac{\partial(\rho_v u_v)}{\partial x} + \frac{\partial(\rho_v v_v)}{\partial y} = 0, \tag{10}$$

and the momentum equations for computation of the velocity components are [31] the x-momentum equation for computing u:

$$\frac{\partial}{\partial t}(\rho_v u_v) + \frac{\partial}{\partial x}(\rho_v u_v u_v) + \frac{\partial}{\partial y}(\rho_v u_v v_v) = \rho_v g_x - \varphi_v \frac{\partial P}{\partial x} + \mu_v \left(\frac{\partial^2 u_v}{\partial x^2} + \frac{\partial^2 u_v}{\partial y^2} \right), \tag{11}$$

y-momentum equation for computing v:

$$\frac{\partial}{\partial t}(\rho_v v_v) + \frac{\partial}{\partial x}(\rho_v u_v v_v) + \frac{\partial}{\partial y}(\rho_v v_v v_v) = \rho_v g_y - \varphi_v \frac{\partial P}{\partial y} + \mu_v \left(\frac{\partial^2 v_v}{\partial x^2} + \frac{\partial^2 v_v}{\partial y^2} \right). \tag{12}$$

The energy equation, neglecting the viscous dissipation term, is used to compute the temperature field:

$$\frac{\partial}{\partial t}(c_v T) + \frac{\partial}{\partial x}(u_v c_v T) + \frac{\partial}{\partial y}(v_v c_v T) = k_v \left(\frac{\partial^2 T}{\partial x^2} + \frac{\partial^2 T}{\partial y^2} \right). \tag{13}$$

For the temperature–pressure relationship in the vapor, the ideal gas equation of state is used:

$$P_v = \rho_v R T. \tag{14}$$

3. Boundary conditions

3.1. Front wall (evaporator side)

$$q''(y) = -k \left. \frac{\partial T}{\partial x} \right|_{x=0}. \tag{15}$$

The heat flux distribution on the front wall was determined by a hybrid experimental and numerical data analysis. The heat flux distribution caused by an impinging propane flame on a flat surface was modeled by a probability function [32]:

$$q''(y) = A \left[1 - \exp\left\{ -\left(\frac{y - L}{L/2} \right)^2 \right\} + B \right]. \tag{16}$$

The coefficients A and B in Eq. (16) were obtained by a comparison of data from the numerical computation and experiments conducted on a solid aluminum plate to yield the temperature distribution on the back side of the plate, the experimental facility used the same configuration as the flat heat pipe as shown in Fig. 1. An iterative procedure was adopted, with an initial assumption of the two constants. The expression for the heat flux distribution was evaluated using an energy balance for the solid aluminum plate subjected to pure heat conduction, with convection and radiation heat transfer at the cold side.

Based on a comparison of the calculated temperature distribution at the back side of the plate with the experimental data, the values of A and B were modified. This iterative process was repeated until the difference between the calculated temperatures and experimental values at the center of the back side were less than or equal to 3.4% for the first 40 s of the transient period. Fig. 3 shows the results of this procedure, where a comparison of the experimental and numerical results for the solid aluminum plate are presented for $t = 40$ s.

3.2. Wall–wick interface

An energy balance at the interface between the flat heat pipe wall and wick yields the following expression, which was used as an interface boundary condition, assuming negligible contact resistance.

$$-k_s \left. \frac{\partial T}{\partial x} \right|_{wall} = -k_w \left. \frac{\partial T}{\partial x} \right|_{wick}. \tag{17}$$

3.3. Liquid–vapor interface

The interfacial density, mass flux and temperature at the vapor core–wick interfaces of the evaporator and condenser are specified below. The vapor is assumed to be fully

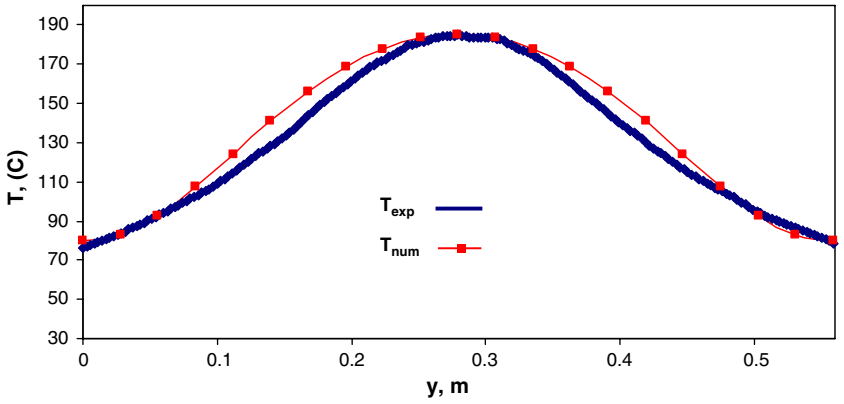

Fig. 3. Comparison of experimental and numerical data for the temperature distribution on the back side of a solid aluminum plate, used in estimating the heat flux distribution at $t = 40$ s.

saturated, and its density is evaluated for the corresponding temperature at the interface. At $x = 0$, $0 \leqslant y \leqslant H/2$.

$$\rho_i = \rho_{sat}(T_v). \tag{18}$$

Several expressions have been proposed in the heat pipe literature to evaluate the mass flux at the interface; some are based on the kinetic theory while others examine energy balances at the interfaces [20,23,33–39]. Ivanosvski et al. [33] suggested that the processes of evaporation from, and condensation on, a liquid surface must be considered from the perspective of kinetic theory. According to Collier [40] the condensation or evaporation process at the interface can be evaluated in the form suggested by Silver and Simpson [41] and referred to as the Kucherov–Rikenglaz equation:

$$j = \left(\frac{2\hat{\sigma}}{2-\hat{\sigma}}\right)\left(\frac{M}{2\pi R}\right)^{1/2}\left[\frac{p_v}{T_v^{1/2}} - \frac{p_l}{T_l^{1/2}}\right]. \tag{19}$$

Eq. (19) is found to be sufficiently valid for low rates of condensation or evaporation, ignoring non-equilibrium interactions between the impinging and departing molecules. Based on this formulation a detailed analysis was performed to obtain a simplified expression for computing the velocity and mass flux at the interface.

If the temperature and pressure of the liquid phase can be expressed in terms of the temperature and pressure differences at the interface as suggested in [42]:

$$p_l = p_v - \Delta p \quad \text{and} \quad T_l = T_v - \Delta T, \tag{20}$$

then Eq. (19) becomes:

$$j = \left(\frac{2\hat{\sigma}}{2-\hat{\sigma}}\right)\left(\frac{M}{2\pi R}\right)^{1/2}\left[\frac{p_v}{T_v^{1/2}} - \frac{p_v - \Delta p}{T_v^{1/2}(1-\Delta T/T_v)^{1/2}}\right]. \tag{21}$$

Eq. (21) has a highly non-linear term containing the vapor temperature, denoted by F:

$$F = \frac{1}{(1-\Delta T/T_v)^{1/2}}. \tag{22}$$

By numerical approximation it is possible to reduce this non-linear function into a simpler linear function G given by:

$$G = 1 + \frac{1}{2}\frac{\Delta T}{T_v}. \tag{23}$$

Fig. 4 shows the non-linear function, F, and the linear function, G, for the interval $0 \leqslant |\Delta T|/T_v \leqslant 0.1$. The maximum error for the linear function G with respect to F at $|\Delta T|/T_v = 0.1$ was found to be 0.388%.

For small pressure differences across the liquid–vapor interface, substituting Eq. (23) into Eq. (21), the following simplified expression can be obtained:

$$j = \left(\frac{2\hat{\sigma}}{2-\hat{\sigma}}\right)\left(\frac{M}{2\pi R T_v}\right)^{1/2}\left[\frac{\Delta p}{\Delta T} - \frac{p_v}{2T_v}\right]\Delta T. \tag{24}$$

By applying the Clausius–Clapeyron equation to Eq. (24), the mass flux at the interface can be obtained as:

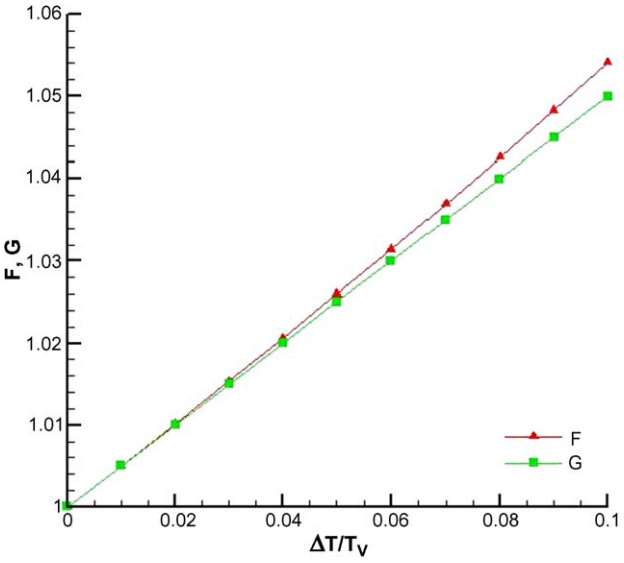

Fig. 4. Linear approximation vs. the non-linear function given by Eq. (22).

$$m_i'' = \frac{2\hat{\sigma}}{2-\hat{\sigma}}\frac{h_{fg}}{T_{sat}v_{fg}}\left(\frac{M}{2\pi R T_{sat}}\right)^{1/2}\left(1 - \frac{P_l v_{fg}}{2h_{fg}}\right)\Delta T. \tag{25}$$

In order to perform the numerical computation, it is more useful to have an expression for the velocity of the vapor at the interface, than to use the mass flux. From the continuity equation at the interface:

$$m_i'' = \rho_i u_i. \tag{26}$$

Combining Eqs. (25), (26), the normal velocity of the vapor at the interface can be expressed as:

$$u_i = \frac{2\hat{\sigma}}{2-\hat{\sigma}}\frac{h_{fg}}{T_{sat}v_{fg}\rho_i}\left(\frac{M}{2\pi R T_{sat}}\right)^{1/2}\left(1 - \frac{P_l v_{fg}}{2h_{fg}}\right)\Delta T. \tag{27}$$

To simplify the analysis, it is assumed that the interface is at the saturation condition ($T_{sat} = T_v$), so that the interfacial density is given by:

$$\rho_i = 1/v_g. \tag{28}$$

Eq. (27) then becomes:

$$u_i = \frac{2\hat{\sigma}}{2-\hat{\sigma}}\frac{h_{fg}}{T_v}\left(\frac{M}{2\pi R T_v}\right)^{1/2}\cdot\left(1 - \frac{v_f(T_v)}{v_g(T_v)}\right)^{-1} \cdot\left[1 - \frac{p_v(T_v)v_{fg}(T_v)}{2h_{fg}(T_v)}\right]\Delta T. \tag{29}$$

In order to simplify the expression in Eq. (29), Ψ is defined as a function which contains only thermodynamic properties, and depends on the vapor temperature:

$$\Psi = h_{fg}(T_v)\cdot\left(1 - \frac{v_f(T_v)}{v_g(T_v)}\right)^{-1}\cdot\left[1 - \frac{p_v(T_v)v_{fg}(T_v)}{2h_{fg}(T_v)}\right]. \tag{30}$$

The function Ψ is shown in Fig. 5, for temperatures between 25 and 160 °C. It was found that this expression gives an almost linear variation, and Ψ can be written in

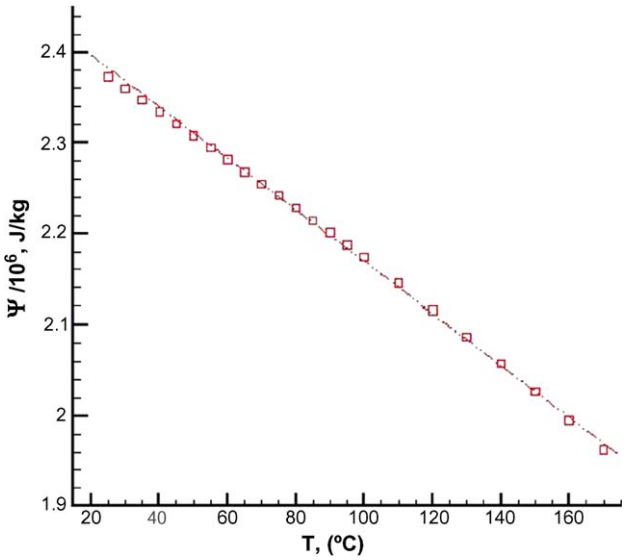

Fig. 5. Linear approximation of Ψ as function of the saturation temperature in the vapor core.

a simplified form using a straight line fitting procedure as follows:

$$\frac{\Psi}{10^6} \simeq (2.4491 - 0.0028\ T_{\mathrm{v}}), \frac{\mathrm{J}}{\mathrm{kg}}. \tag{31}$$

This linearization simplifies the expression for the velocity of vapor at the interface, given in Eq. (29), as follows:

$$u_{\mathrm{i}} = \frac{2\hat{\sigma}}{2-\hat{\sigma}} \frac{\Psi}{T_{\mathrm{v}}} \left(\frac{M}{2\pi R T_{\mathrm{v}}}\right)^{1/2} \Delta T. \tag{32}$$

It is apparent from Eq. (32) that the interfacial vapor velocity is inversely affected by the vapor temperature. This with Eq. (26) also indicates that the velocity at the interface is influenced by the thermodynamic function Ψ, which depends on the vapor temperature. The following equation is used in combination with Eqs. (28) and (32):

$$c_{\mathrm{i}} \frac{V_{\mathrm{i}}}{A_c} \frac{\mathrm{d}T}{\mathrm{d}t} = -k_{\mathrm{w}} \left.\frac{\partial T}{\partial x}\right|_{\mathrm{l-i}} + m''_{\mathrm{i}} h_f + k_{\mathrm{v}} \left.\frac{\partial T}{\partial x}\right|_{\mathrm{i-v}} - m''_{\mathrm{i}} h_g, \tag{33}$$

and the pressure at the interface can be calculated using the Clausius–Clapeyron equation:

$$p_{\mathrm{i}} = p_{\mathrm{v}} \exp\left[\frac{h_{fg}}{R_{\mathrm{v}}}\left(\frac{1}{T_{\mathrm{v}}} - \frac{1}{T_{\mathrm{i}}}\right)\right]. \tag{34}$$

3.4. Other boundary conditions at the vapor core

At $0 \leqslant x \leqslant W$, $y = H/2$

$$\left.\frac{\partial T}{\partial x}\right|_{y=H/2} = 0, \tag{35}$$

$$u = v = \frac{\partial \rho}{\partial y} = 0. \tag{36}$$

At $0 \leqslant x \leqslant W$, $y = 0$

$$\frac{\partial(\Gamma)}{\partial y} = 0, \tag{37}$$

where Γ represents the convective terms in the y-direction in the continuity, momentum and energy equations given byρu, ρuv, and ρcvT, respectively.

3.5. Boundary condition at the back wall

The heat transfer from the external surface of the back wall is due to convection and radiation. For the radiative portion, it is assumed that the outside surface of the back wall behaves as a black body. The boundary condition at the back wall was assumed to be a black body with natural convection, which provides the cooling for the surface. The convective heat transfer coefficient and the ambient temperature were assumed to be constant:

$$-k \left.\frac{\partial T}{\partial x}\right|_{x=w} = h(T - T_\infty) + \varepsilon \sigma_R (T^4 - T_\infty^4). \tag{38}$$

3.6. Initial conditions

The initial conditions were assumed for a saturated vapor and uniform temperature and pressure fields. It was also assumed that the initial velocities were zero. These conditions are stated below.

At $t = 0$:

$$T_0 = 26.3\ ^\circ\mathrm{C}, \quad P_{\mathrm{sat}} = P(T_0), \quad \rho_{\mathrm{v}} = \rho_{\mathrm{v}}(T_0), \quad \rho_{\mathrm{l}} = \rho_{\mathrm{l}}(T_0) \tag{39}$$

and

$$u = v = 0. \tag{40}$$

4. Numerical solution

4.1. Computational scheme

In order to capture the transient variations with minimal round-off errors, and also to simplify the computational scheme, an explicit computational procedure was employed. The physical domain was discretized into a 40×100 mesh, utilizing unequal grids in the x and y-directions, consistent with the physical dimensions of the flat heat pipe. This produced a spatial grid size of 0.00127 m, 0.00044 m and 0.0023 m in the x-direction in the wall, wick and vapor core, respectively, and 0.002794 m in the y-direction. The time step required for convergence was determined to be 0.00001 s using a trial and error process. To overcome the instabilities in the vapor core, successive under-relaxation was applied to the velocities and temperatures computed at each time step.

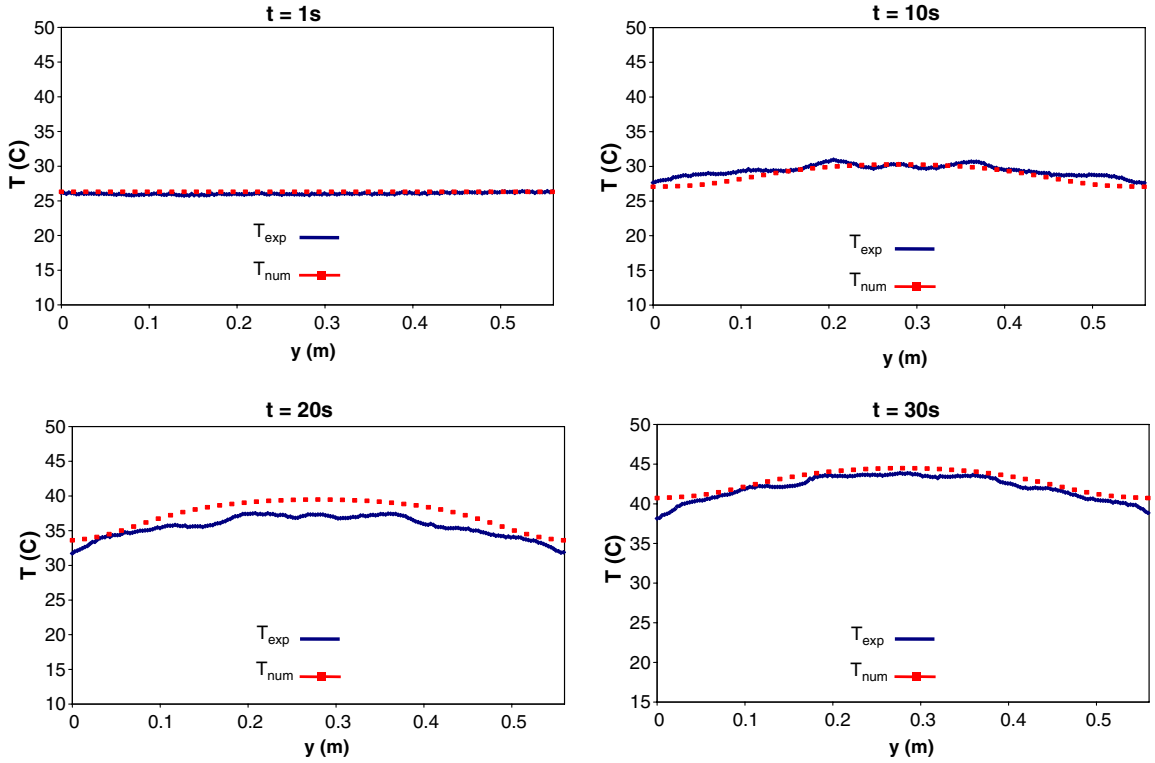

Fig. 6. Validation of computational results by comparison with experimental results at the back side of the flat heat pipe at times $t = 1$, 10, 20 and 30 s.

4.2. Experimental validation of computational results

Experimental data were obtained for the configuration shown in Fig. 2. An infrared thermal imaging camera located at the back side of the panel registered the temperature field on that surface. The infrared camera was carefully calibrated with a margin of error of ±0.5 °C. The camera recorded temperature data at 1 s intervals during the heating process. Both experimental and numerical data are shown in Fig. 6, and as indicated, agree reasonably well during the transient time period analyzed.

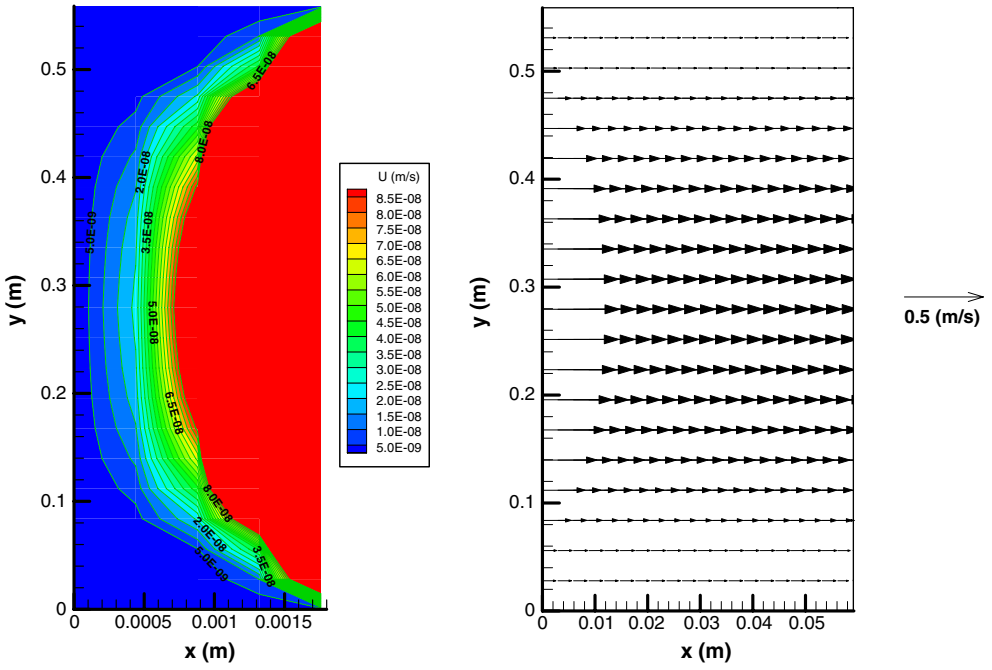

Fig. 7. Velocity contours in the front (evaporator side) wick and velocity vector plot for the vapor core at $t = 10$ s.

Modeling the transient performance of a heat pipe is a challenging problem, especially when the phase change at the liquid–vapor interface and the radiative heat transfer are included in the analysis. Fig. 6 shows that the numerical data is in good agreement with the experimental data. Initially the temperature is constant and uniform throughout the back panel, where as time progresses, it increased. After a slight non-uniformity due to early transient effects observed in the first 20 s, the temperature distribution again becomes reasonably uniform throughout the surface (as at $t = 30$ s). Convective and radiative effects were considered on the back side, with the assumption of the surface acting as a black body.

5. Results and discussion

Given the reasonable agreement between the model and experiments, the model can now be used to investigate the effect of a non-uniform input heat distribution on the performance of a flat heat pipe. The temperature distribution at the cold, i.e., the back side of the plate, the temperature field in the system and the velocity distribution in the wick and vapor core regions are the primary indicators of the flat heat pipe performance. The phase change at the liquid–vapor interface results in a complex numerical convergence problem. Additionally, the analysis of the vapor core using a conservative formulation to compensate for the effects of mass addition and depletion causes instabilities and the associated divergence. The analyzed process corresponds only to a highly transient period of operation of the flat heat pipe, which means that the mass flow rates at the evaporator and condenser are essentially unequal. Some of the mass added at the evaporator remains as vapor, whereas some of it condenses in the cold regions. Details of the numerical results are presented and discussed in Figs. 7–10.

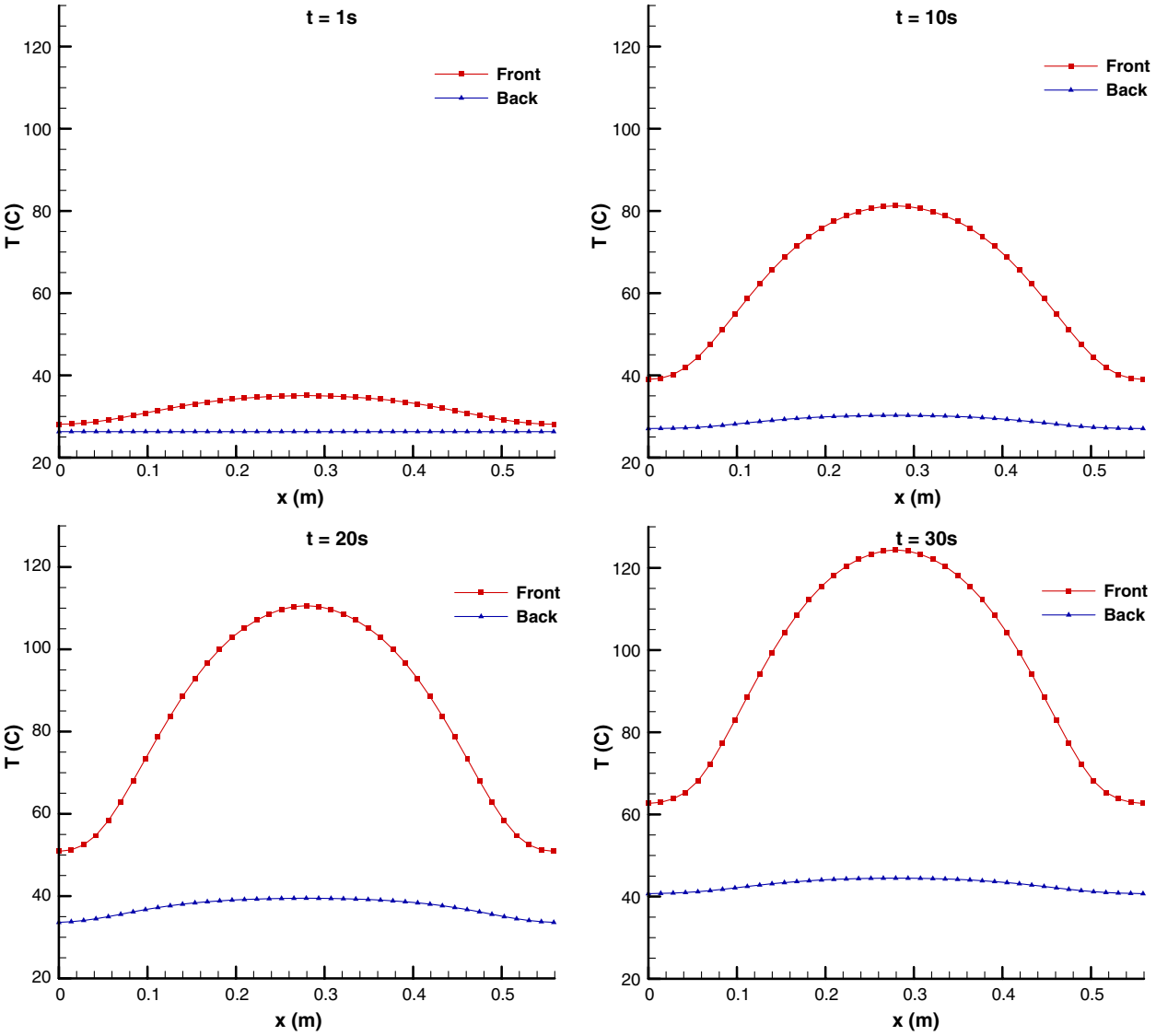

Fig. 8. Temperature distribution on the front and back sides of the flat heat pipe at times of 1, 10, 20 and 30 s.

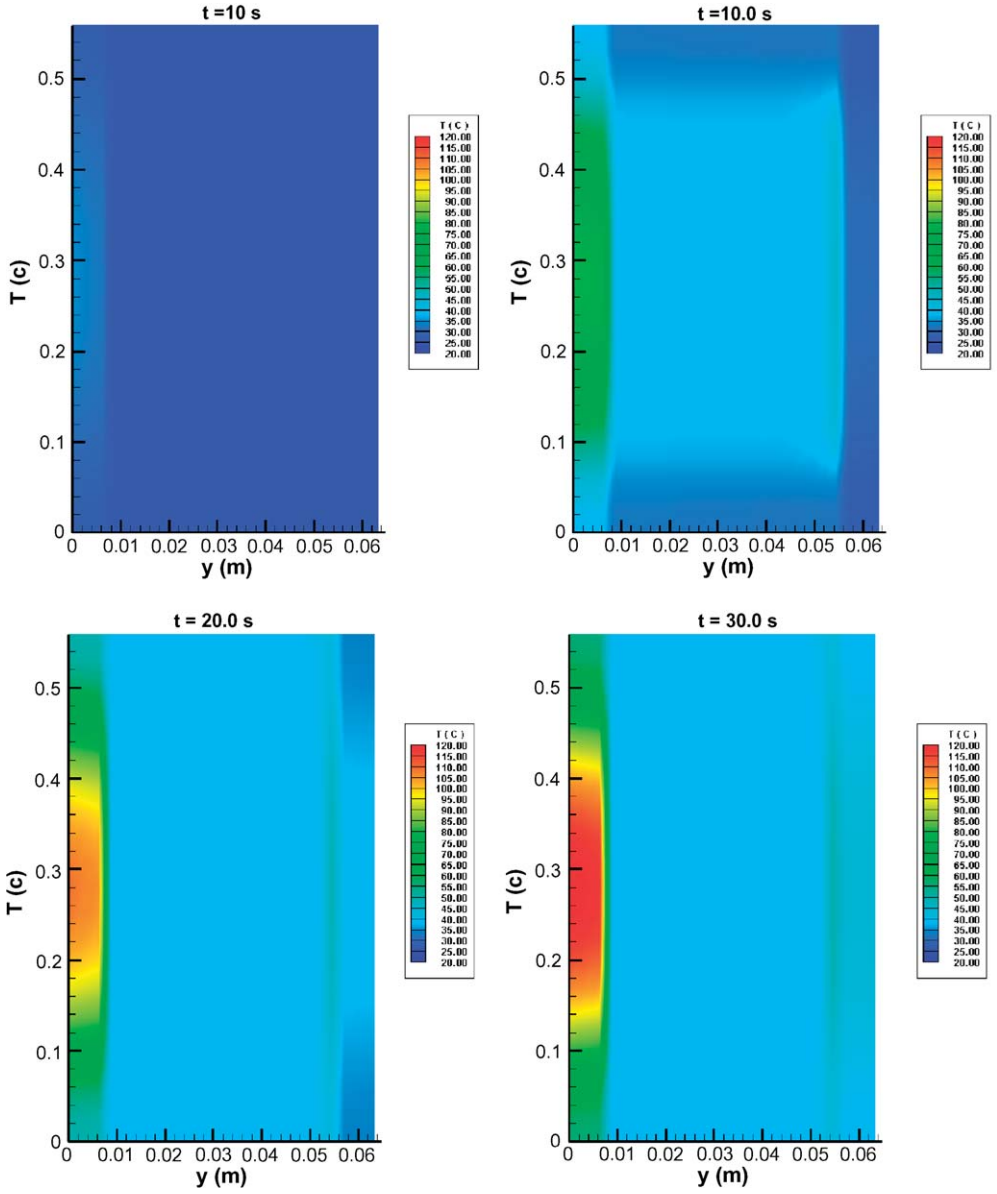

Fig. 9. Temperature distribution across the flat heat pipe at times of 1, 10, 20 and 30 s.

The effect of the vaporization rate at the interface between the wick and vapor core at $t = 10$ s is shown in Fig. 7. The results indicate that the velocities are small in the wick. In contrast, the velocity in the vapor core is several orders of magnitude higher than that in the wick; with the effect being characteristic of the densities of the two phases of the working fluid. Continuous vaporization at the interface induces the velocity field in the vapor core; in the present case the vapor generation was modeled using kinetic theory, under the assumption of a moderate temperature drop at the interface (Eq. (32)). At the interface, the liquid–vapor temperature difference is indirectly determined by the non-uniform input heat transfer rate.

The temperature distribution obtained from the computation, at the hot (front) and the cold (back) faces of the flat heat pipe heat spreader, at 1, 10, 20, 30 s, are presented in Fig. 8. The temperature distribution at the hot side is non-uniform due to the applied non-uniform heat input, and its magnitude increases with respect to time. At the back side of the flat heat pipe, the temperature distribution is much more uniform, which is essentially what is expected from the use of the flat heat pipe. The phase change process and the resulting heat pipe effect inside the system are responsible for the uniform distribution obtained at the cold side of the device. This flattening of the temperature distribution at the condenser side makes it possible to cool this face effectively using an external coolant since the heat can be dissipated over the entire surface, allowing the entire back surface to be used in the heat rejection process.

At the evaporator, the conversion of the working fluid from the liquid to the vapor phase requires that a considerable amount of energy be transferred from the working

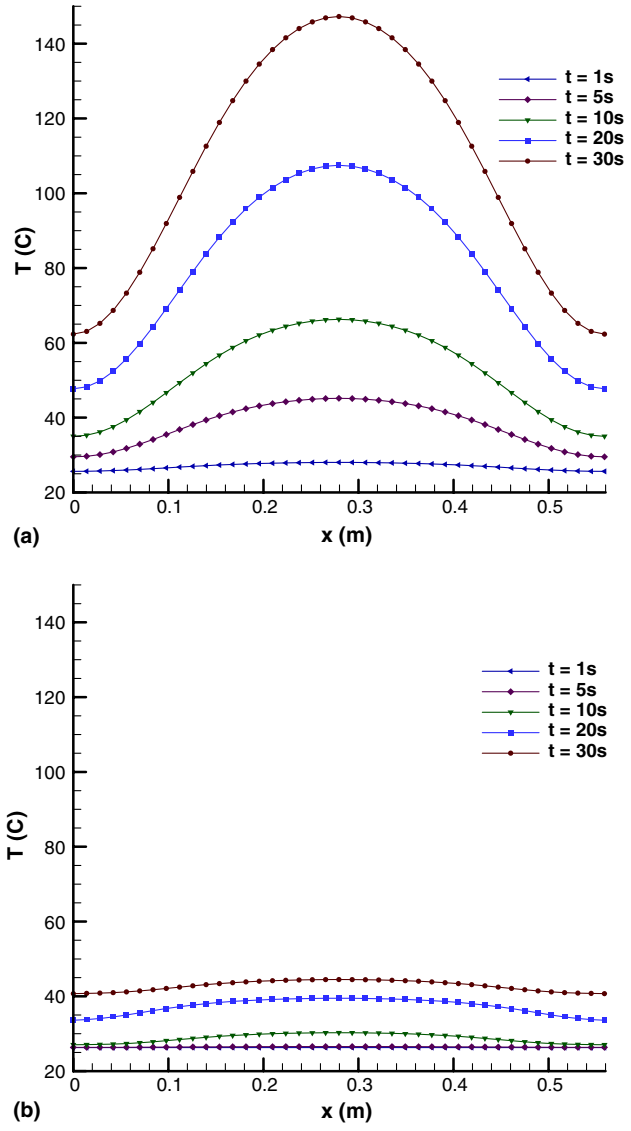

Fig. 10. Temperature profiles (a) at the back side of an aluminum flat plate subjected to the same boundary conditions as the flat heat pipe, (b) at the back side of the flat heat pipe.

fluid to the vapor. The velocity imparted to the vapor assists in this energy transport from the evaporator to the condenser. The combined effect of the phase change and fluid transport in the vapor core makes the flat heat pipe operational. The condensation process in the wick at the back side of the heat spreader, which takes place at an almost uniform temperature, allows the condenser side of the heat spreader to attain a more or less uniform external temperature.

Fig. 9 illustrates the temperature contours across the flat heat pipe at times of 1, 10, 20 and 30 s. As illustrated, the hottest region is located at the center of the front side, where the non-uniform heat is applied. A significant temperature drop is observed in the wick as a result of the small effective thermal conductivity and heat capacity of the metal foam wick, compared to the aluminum wall. Initially, the temperature difference in the vapor core is appreciable, but as the process continues it becomes more uniform. The fluid transport improves as the process proceeds in time, inducing a clear distribution of temperature in the vapor core. The contour plot of the temperature field reveals that the heat rejection at the condenser side is at an almost uniform temperature. Fig. 8 shows more details of the temperature distribution at the cold side of the heat spreader.

A comparison can be made between the flat heat pipe and a mass equivalent solid plate, of the temperature distribution on the back side. An appreciable difference is observed in the temperature distribution on the back side for a solid plate and flat heat pipe. In the case of the solid plate, Fig. 10(a), heat is only transferred by conduction and the temperature distribution on the back side follows a similar pattern as the front side, where an obvious peak is observed at the center. Alternatively, the temperature distribution on the back side of the flat heat pipe, Fig. 10(b), is much flatter than that of the solid plate, and is distinctly different than that of the front side, indicating that significant thermal spreading has occurred. In addition, the use of a phase change in the working fluid results in a tremendous thermal capacity, which helps to maintain the temperature at a relatively low level for the heat flux applied.

6. Conclusions

A mathematical model of heat transfer and fluid flow in a flat heat pipe was developed and used to evaluate the effects of a non-uniform input heat flux distribution, on the temperature and velocity fields within the thermal spreader. The analysis of the flat heat pipe included the wall, wick and vapor core components. The analysis was performed for the early transient response of the flat heat pipe design. A constant non-uniform heat flux was modeled at the evaporator side and a constant heat transfer coefficient at the condenser side was assumed. The model also incorporated radiative cooling from the heat spreader wall.

The numerical results were compared with experimental data and good agreement was observed. It was found that the temperature distribution on the back side of the flat heat pipe was uniform, indicating the thermal spreading effects of the flat heat pipe.

Acknowledgements

The authors would like to acknowledge joint support from the Defense Advanced Research Projects Agency and the Office of Naval Research under grant number N00014010454 and the support of the National Science Foundation through grant number CTS-0312848. DARPA Distribution Statement A: Approved for public release.

References

[1] T.P. Cotter, Theory of Heat Pipes, Los Alamos National Laboratory Report No. LA-3246-MS, The University of California, Los Alamos, NM, 1964.

[2] D.J. Dean, Integral heat pipe package for microelectronic circuits, Adv. Environ. Sci. Technol. (1) (1976) 481–502.

[3] A. Itoh, Micro Heat Pipes, Prospectus of the Itoh R and D Laboratory, Osaka, Japan, 1988.

[4] J.M. Modlin, G.T. Colwell, Surface cooling of scramjet engine inlets using heat pipe, transpiration, and film cooling, J. Thermophys. Heat Transfer 6 (3) (1992) 500–504.

[5] A. Bontemps, C. Goubier, C. Marquet, J.C. Solecki, Theoretical analysis of a revolving heat-pipe, in: Proceedings of the Fifth International Heat Pipe Conference, Tsukuba Science City, Japan, 1984, pp. 274–279.

[6] G.P. Peterson, Investigation of miniature heat pipes, Final Report, Wright-Patterson Air Force Base, Contract No. F33615-86-C-2723, Task 9 (1988b).F.

[7] Song, D. Ewing, C.Y. Ching, Experimental investigation on the heat transfer characteristics of axial rotating heat pipes, Int. J. Heat Mass Transfer 47 (22) (2004) 4721–4731.

[8] A. Merlone, R. Dematteis, P. Marcarino, Gas-controlled heat pipes for accurate liquid–vapor transition measurements, Int. J. Thermophys. 24 (3) (2003) 695–712.

[9] S.V. Garimella, C.B. Sobhan, Recent advances in the modeling and applications of nonconventional heat pipes, Adv. Heat Transfer, vol. 35, Academic Press, New York, 2001, pp. 249–308.

[10] K. Take, Y. Furukawa, S. Ushioda, Fundamental investigation of roll bond heat pipe as heat spreader plate for notebook computer, IEEE Trans. Comp. Pack. Technol. 23 (1) (2000) 80–85.

[11] S. Kalahasti, Y.K. Joshi, Performance characterization of a novel flat plate micro heat pipe spreader, IEEE Trans. Comp. Pack. Technol. 25 (4) (2002) 554–560.

[12] Y. Avenas, C. Gillot, A. Bricard, C. Schaeffer, On the use of flat heat pipes as thermal spreaders in power electronics cooling, IEEE Annual Power Electron. Specialists Conf. 2 (2002) 753–757.

[13] C. Gillot, A. Lai, M. Ivanova, Y. Avenas, C. Schaeffer, E. Fournier, Experimental study of a flat silicon heat pipe with microcapillary grooves, in: Thermomechanical Phenomena in Electronic Systems, Proceedings of the Intersociety Conference on Thermal and Thermomechanical Phenomena in Electronic Systems, 2004, pp. 47–51.

[14] H. Van Ooijen, C.J. Hoogendoorn, Vapor flow calculation in a flat heat pipe, AIAA J. 17 (11) (1979) 1251–1259.

[15] A. Faghri, Vapor flow analysis in a double walled concentric heat pipe, Numer. Heat Transfer 10 (6) (1986) 583–595.

[16] A. Faghri, Performance characteristic of a concentric annular heat pipe, part II: vapor flow analysis, ASME Heat Transfer Div. 96 (1988) 389–396.

[17] M.M. Chen, A. Faghri, An analysis of the vapor flow and the heat conduction through the liquid wick and pipe wall in a heat pipe with single or multiple heat sources, Int. J. Heat Mass Transfer 33 (9) (1990) 1945–1955.

[18] F. Issacci, I. Catton, N.M. Ghoniem, Vapor dynamics of heat pipe start-up, J. Heat Transfer 113 (1991) 985–994.

[19] J.H. Jang, A. Faghri, W.S. Chang, Analysis of the one-dimensional transient compressible vapor flow in heat pipes, Int. J. Heat Mass Transfer 34 (8) (1991) 2029–2037.

[20] J.M. Tournier, M.S. El-Genk, Heat pipe transient analysis model, Int. J. Heat Mass Transfer 37 (5) (1994) 753–762.

[21] Y. Wang, K. Vafai, Transient characterization of flat plate heat pipes during startup and shutdown operations, Int. J. Heat Mass Transfer 43 (15) (2000) 2461–2655.

[22] Z.J. Zuo, A. Faghri, Network thermodynamic analysis of the heat pipe, Int. J. Heat Mass Transfer 41 (11) (1998) 1473–1484.

[23] U. Vadakkan, J.Y. Murthy, S.V. Garimella, Transient analysis of flat heat pipes, in: Proceedings of the 2003 ASME Summer Heat Transfer Conference, HT2003-47349, Las Vegas, NV, USA, 2003, pp. 1–11.

[24] Y. Xuan, Y. Hong, Q. Li, Investigation on transient behaviors of flat plate heat pipes, Exp. Thermal Fluid Sci. 28 (2004) 249–255.

[25] D.T. Queheillalt, G. Carbajal, G.P. Peterson, H.N.G. Wadley, A truncated honeycomb core heat plate sandwich panel structure, Int. J. Heat Mass Transfer, to be submitted.

[26] J.W. Paek, B.H. Kang, S.Y. Kim, J.M. Hyun, Effective thermal conductivity and permeability of aluminum foam metal, Int. J. Thermophys. 21 (2) (2000) 453–464.

[27] M. Kaviany, Principles of Heat Transfer in Porous Media, Springer Verlag, New York, 1995, p. 67.

[28] G.P. Peterson, An Introduction to Heat Pipes – Modeling, Testing and Applications, Wiley, New York, 1994, pp. 47–48.

[29] A. Bhattacharya, V.V. Calmidi, R.L. Mahajan, Thermophysical properties of high porosity metal foams, Int. J. Heat Mass Transfer 45 (2002) 1017–1031.

[30] A. Bejan, D.A. Nield, Convection in Porous Media, Springer Verlag, New York, USA, 1992.

[31] J.D. Anderson, Computational Fluid Dynamics, McGraw-Hill Inc., New York, 1995.

[32] J.J. Tuma, Engineering Mathematics Handbook, McGraw-Hill Book Company, New York, 1979.

[33] M.N. Ivanovskii, V.P. Sorokin, I.V. Yagodkin, The Physical Principles of Heat Pipes, Clarendon Press, Oxford, 1982, pp. 116–118.

[34] D. Wu, G.P. Peterson, Investigation of the transient characteristics of a micro heat pipe, J. Thermophys. Heat Transfer 5 (2) (1991) 129–134.

[35] G.P. Peterson, An Introduction to Heat Pipes – Modeling, Testing and Applications, Wiley, New York, 1994, pp. 67–68.

[36] M.J. Tournier, M.S. El-Genk, A vapor flow model for analysis of liquid-metal heat pipe startup from a frozen state, Int. J. Heat Mass Transfer 39 (18) (1996) 3767–3780.

[37] D. Khrustalev, A. Faghri, Estimation of the maximum heat flux in the inverted meniscus type evaporator of a flat miniature heat pipe, Int. J. Heat Mass Transfer 39 (9) (1996) 1899–1909.

[38] C.B. Sobhan, S.V. Garimella, V.V. Unnikrishnan, A computational model for the transient analysis of flat heat pipe, in: Thermomechanical Phenomena in Electronic Systems, Proceedings of the Intersociety Conference, vol. 2, 2000, pp. 106–113.

[39] G.V. Kutznetsov, A.E. Sitnikov, Numerical analysis of basic regulations of heat and mass transfer in a high-temperature heat pipe, High Temp. 40 (6) (2002) 898–904.

[40] J.G. Collier, Convective Boiling and Condensation, Mc-Graw Hill, London, 1972.

[41] R.S. Silver, H.C. Simpson, The condensation of superheated steam, in: Proceedings of a Conference held at the National Engineering Laboratory, Glasgow, Scotland, 1961.

[42] V.P. Carey, Liquid–Vapor Phase-Change Phenomena, Taylor & Francis, USA, 1992.